Extracting heat energy through the road pavement: a novel solution with porous concrete

Domenico Vizzari, Eric Gennesseaux, Jean Dumoulin, Emmanuel Chailleux, Stephane Lavaud, Jean-Luc Manceau, Thierry Sedran

EXTRACTING HEAT ENERGY THROUGH THE ROAD PAVEMENT: A NOVEL SOLUTION WITH POROUS CONCRETE

Domenico Vizzari, University Gustave Eiffel, MAST/MIT, F-44340 Bouguenais, France
domenico.vizzari@univ-eiffel.fr

Eric Gennesseaux, University Gustave Eiffel, MAST/MIT, F-44340 Bouguenais, France
eric.gennesseaux@univ-eiffel.fr

Jean Dumoulin, University Gustave Eiffel, COSYS/SII, F-44340 Bouguenais, France
jean.dumoulin@univ-eiffel.fr

Emmanuel Chailleux, University Gustave Eiffel, MAST/MIT, F-44340 Bouguenais, France
emmanuel.chailleux@univ-eiffel.fr

Stephane Lavaud, University Gustave Eiffel, MAST/MIT, F-44340 Bouguenais, France
stephane.lavaud@univ-eiffel.fr

Jean-Luc Manceau, University Gustave Eiffel, COSYS/SII, F-44340 Bouguenais, France
jean-luc.manceau @univ-eiffel.fr

Thierry Sedran, University Gustave Eiffel, MAST/MIT, F-44340 Bouguenais, France
thierry.sedran@univ-eiffel.fr

ABSTRACT

The sun is by far the largest source of clean energy and the road network is daily exposed to this big amount of radiation. At present, the solar radiation can be directly converted into electrical power thanks to the photovoltaic effect, or harvested by means of a heat-transfer fluid. This paper deals with the second solution, proposing a multilayer road system able to exploit the thermal gradient of the pavement.
The system is composed of a porous core, sandwiched between two layers. The base layer is waterproof and it contributes to the mechanical performance of the entire system; the core is a porous concrete mixture for the circulation of the heat-transfer fluid and it works as a solar collector and the top layer is a semi-transparent material designed to support the traffic vehicles, guarantee the skid resistance and maximize the harvested energy.
At first, the authors worked on the mix-design of the porous core and of the semi-transparent layer. Secondly, they built a working prototype in order to evaluate harvested heat energy in lab-condition.
In comparison to the state-of-art, the results show a clear improvement in terms of energy harvesting, leading the way for the construction of a full-scale prototype and a comprehensive evaluation in-situ conditions.

KEY WORDS

ENERGY HARVESTING / POROUS CONCRETE / MIX-DESIGN / LAB-SCALE PROTOTYPE/ PAVEMENT

1. INTRODUCTION

“Energy-related CO_2 emissions increase 6% from 33 Gt in 2015 to 35 Gt in 2050 under current and planned policies” and, at the same time, “emissions need to fall to 9.7 Gt in 2050 for an emissions pathway compatible with the 2 °C target of the Paris Agreement” (Gielen et al., 2019). In this scenario, renewable energies play a primary role towards the objective of net-zero emissions. Among all the renewable energies, the sun is by far the largest source. According to Lewis (Lewis,

2005), if 0.16% of the land on Earth would be covered by solar cells having 10% of efficiency, that would produce the equivalent of 20'000 1-GWe nuclear fission plants, roughly corresponding to global demands for carbon-neutral energy.
The road network is daily exposed to the sunlight radiation and it can coexist with some energy harvesting technology. According to (Meijer, 2018), the total length of the pavements in the world is around 22 million km; assuming an average width of 6 m for the roads, the total surface would be around 0.25% of the land on Earth, which is comparable with Lewis's results.
The solar radiation intercepted by the road network could be converted into electricity through the solar cells, or it could be harvested through a heat-exchange fluid, based on the principle of the solar thermal collectors.
Obviously, the adding of these new features requires to re-think the design, the manufacture, the installation and the maintenance of the road infrastructure.
To this end, academia and industry focalize on two main solutions: the photovoltaic pavement and the asphalt solar collectors (Vizzari et al., 2021).
The photovoltaic pavement are able to generate electricity thanks to the solar cells.
The structural type from top to bottom is given by the semi-transparent layer, the electric layer and the bearing layer.
The semi-transparent layer is usually toughened glass, high molecular polymer (polycarbonates, PMMA), or a mixture of transparent glue and glass aggregates.
The electric layer contains the solar cells and it is covered/merged with the semi-transparent layer. It can integrate LED lights for road marking, heating elements to de-ice the surface or sensors to detect the traffic volume or the weather conditions.
Finally, the bearing layer is a concrete or bituminous base, able to transfer the traffic load to the soil (Hu et al., 2022).
The asphalt solar collectors consist on a series of pipes embedded into the asphalt. The solar radiation is firstly absorbed by the asphalt pavement. In return, the solar radiation causes the increase of temperature in the pavement, leading to a conduction phenomenon from the surface to the lower layers of the road. The conduction involves also the asphalt-pipes interface. Finally, the heat is transferred to the water (or other heat carrier fluid) thanks to the convection between pipes and fluid. In summer, the solar energy collected from the asphalt pavement can be stored in boreholes and re-use during winter for de-icing the surface, or to power a heat pump for the heating of buildings.
Depending on the heat-transfer properties of the pavement, the disposition/dimension of the pipes (length, depth, spacing, pipe diameter), the inlet temperature of the water and the speed, the efficiency of the system can change. The Table 1 shows an extract of the most significant results in the state-of-art.

Table 1 – State of art for asphalt solar collectors

Author	**Material**	**Embedded depth**	**Embedded spacing**	**Pipe diameter**	**Source radiation**	**ΔT inlet-outlet**	**Flow rate**	**Harvested energy**	**Efficiency**
Shaopeng et al., 2011	Asphalt mixture	5 cm	10 cm	2 cm	Lab condition : 1200 W/m^2	0.39 – 1.8 °C	54 – 1886 ml/min	400 – 450 W/m^2	0.33
Gao et al., 2010	Cement concrete	1 cm	9, 12 and 15 cm	2 cm	Real condition : 0 – 800 W/m^2	0.293, 0.27 and 0.178 °C/m	70, 80 and 100 l/h	150 -250 W/m^2	Up to 0.3
Yan et al., 2009	Asphalt mixture (Thermal conductivity 1.2, 1.6, 2 and 2.4 W/mK)				Early autumn in the Changch un city at 13:00	0.196, 0.056, 0.021 and 0.013 °C/m	0.1, 1, 3, 5 m/s (fluid velocity)	260 – 280 W/m^2	
Van	Asphalt	7 cm	5 – 50	2 cm	1000		0.04 –	≈ 210	0.21

Bijsterveld et al., 2001	mixture		cm		W/m^2		0.5 l/s	W/m^2	
Ao et al., 2016	Asphalt mixture (thermal conductivity 2.5 W/mK)	1 – 3 cm	10 -20 cm	1-3 cm	Jeddah city, from May to Sept		875 l/h	88 – 198 W/m^2	0.096 – 0.25
Siebert & Zacharakis, 2010	Asphalt mixture	5 cm	20 cm	5 cm			3 l/s		0.38

It is worth to note how the efficiency of the systems is, on average, 0.26. Even optimizing the pipes design, the intrinsic limit remains the poor water flow passing through the collectors.
Moving from this observation, some researchers propose to replace the collectors with a porous asphalt. The logic is that by increasing the permeability of the medium and the contact surface between water and medium, the harvested energy increases. In other terms, the higher is the hydraulic conductivity, the higher is the collected energy. Table 2 shows the main results of literature. In general, the porous medium is asphalt mixture, having porosity between 0.2 and 0.3 and thickness between 4 and 8 cm.

Table 2 – State of art for porous asphalt as active solar collector

Author	Material	Porosity	Thickness	Solar radiation	Flow rate	Harvested energy	Efficiency
Pascual-Muñoz, et al., 2013	Porous asphalt mixture	0.23, 0.27	4 cm	300, 373 and 440 W/m^2	0.005 – 0.02 l/s (after 6 hours)		0.45, 0.40 and 0.35 (porosity = 0.23); 0.85, 0.80 and 0.75 (porosity = 0.27)
Le Touz et al., 2018	Porous asphalt mixture		8 cm	786 – 1035 KWh/m2 (from May to October)		261 – 424 (asphalt course) 320 – 500 kWh/m^2 (from October to May)	0.311 – 0.395 (asphalt course) 0.382 – 0.483 (semi-transparent layer)
Asfour et al., 2016	Porous asphalt mixture	0.2	8 cm	* the input is the temperature injection of the water: 15°C	62.5; 125; 187.5 and 250 l/h	125-270 W/m^2	

Excluding the highest values of efficiency, the average is around 0.38, which is still 47% higher than the asphalt solar collectors. However, the state-of-art is limited to the asphalt mixture. The novelty of this paper is to propose a new prototype for the energy harvesting, in which the asphalt mixture is replaced by the porous concrete, able to reach greater porosity and permeability. Furthermore, the top layer is a photovoltaic road, which is able to generate electricity and maximize to the overall efficiency.

2. THE PROTOTYPE: WORKING PRINCIPLE, MATERIALS AND DIMENSIONS

The prototype is a multi-layer structure able to generate electricity thanks to the solar cells and to harvest the exceeding heat of the pavement through the water.
The energy is firstly balanced along the interface surface-atmosphere. The resulting heat flux is given by the incident solar radiation, by the convection between surface and air and by the thermal radiation of the prototype. In return, the heat flux provokes an increase of temperature in the prototype (thermal diffusion). Finally, a convection mechanism takes place in the interface between the porous concrete and the fluid.

From the top to the bottom, the prototype is composed by: i) 1-cm of semi-transparent layer of glass aggregates and transparent polyurethane, spread according to the surface dressing technique; ii) three independent solar cells iii) 0.5 cm of concrete mortar, specifically designed to have a flat surface to host the solar cells and a sufficient viscosity to not pour into the porous medium; iv) 7 cm of porous concrete for the circulation of the heat transfer fluid; v) a second layer of concrete mortar, to facilitate the casting of the porous concrete and improve the waterproofing; vi) 4.5 cm of concrete base (Figure 1).

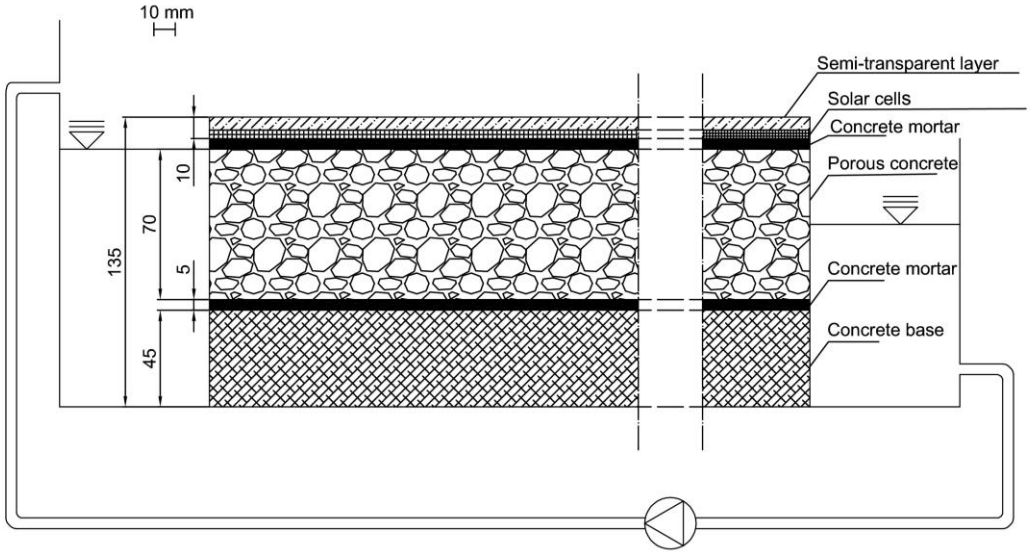

Figure 1 – Sketch of the prototype (in mm)

The mix design and some characteristics of the concrete are summarized in Table 3. Depending on the use of the concrete, the mix-design incorporates the strength (concrete base), the porosity (porous concrete) and the workability (concrete mortar). It can be noted here that the concrete base was not optimized for traffic in this specific case, where only an energetic evaluation of the prototype is proposed.

Table 3 – Mix-design of concrete base, porous concrete and concrete mortar

	Concrete base	**Porous concrete**	**Concrete mortar**
Water [kg/m^3]	179,7	110	289
Cement CEM I 52,5 [kg/m^3]	302,2	402.1	651
Limestone Filler [kg/m^3]	177,9		
0/2 mm sand [kg/m^3]			1300
0/4 mm sand [kg/m^3]	861,6		
5.6/11.2 mm aggregates [kg/m^3]	728,2		
10/14 mm aggregates [kg/m^3]		1361	
Glenium 21 (superplasticizer) [kg/m^3]	3		2.5
MasterAir104DIL (0,2% cement weight) [Kg/m^3]	0,6		
Slump-flow test (cm x cm)	73x71		
Compressive strength Rc at 28 days [MPa]	21.1	7.12	54.4
Indirect tensile strength Rtb at 28 days [MPa]	2.38		
Elastic modulus at 28 days [MPa]	36490		27266

The solar cell is a monocrystalline silicon with dimensions 11cm*11cm*0.3cm. For a solar radiation of 1000 W/m^2 in lab condition, the peak power is 0.95 W, the open circuit voltage Voc is 3.61 V and the short circuit current Isc is 0.39 A.

The semi-transparent layer is a mixture of transparent glue and glass aggregates. The transparent binder is a thermoset polyurethane. It is obtained by mixing two components: the diisocyanate, called component α (containing two or more –NCO groups) and the polyfunctional hydroxy

compounds, called component β (containing the –OH group). The properties of the polyurethane are listed in Table 4 (Vizzari et al., 2020).

Table 4 – Main properties of the polyurethane

Part	Boiling Point (°C)	Flash Point (°C)	Viscosity (mPa s)	Density (gr/cm^3)	Mass Fraction (%)
α	200	70	600 (20 °C)	1.3	58.7
β	200	200	1000 (20 °C)	1.13	41.3

The manufacture of the semi-transparent is inspired by the surface dressing treatment. At first, 0.2 cm of polyurethane is laid down on the solar cells, in order to protect them from punching and obtain a uniform, flat surface; once the first layer of glue completes the polymerization, 2kg/m^2 of 2/4mm glass aggregates are uniformly spread on a second thin layer of polyurethane (0.9 kg/m^2). The compaction is very low and it is carried out immediately after the spreading of the aggregates. The purpose of the compaction is to ensure the penetration and the uniform disposition of the aggregates, before the polymerization of the glue is triggered (Vizzari et al., 2021).

3. MIX-DESIGN OF THE POROUS CONCRETE AND THE CEMENTITOUS MORTAR

During her PhD work, Asfour (Asfour, 2016) designed a porous asphalt mixture presenting a permeability of about 2 cm/s. The author, as well as Le Touz (Le Touz et al., 2018) pointed out that a higher permeability would permit a better efficiency of the system. Some authors have proved a correlation between the permeability of porous concrete and its void ratio in the case of mixes made of the same constituents (Sonebi, 2016). Consequently, a specific study on the porous concrete was carried out in order to maximize its permeability.
Several mix designs of porous concrete were generated from the same aggregates available in different fractions. Those mixtures were tested presenting differences in void ratio (from 15% to 35%) and maximum aggregates diameters (from 4 mm to 14 mm). Higher aggregates diameter was not considered since the width of the porous layer was limited to 10 cm.
Table 5 presents the mix design of the porous concretes tested.

Table 5 – Mix design of the tested mixtures

	BP-0-4-25%	BP-0-4-20%	BP-0-10-25%	BP-0-10-20%	BP-0-4-15%	BP-0-14-3
Cement CEM I 52,5 [Kg/m^3]	398.9	414.8	407.3	420.3	434.8	364.0
0/2 mm sand [Kg/m^3]	0.0	356.3	0.0	361.0	410.8	0.0
2/4mm sand [Kg/m^3]	1350.2	1052.9	0.0	0.0	1067.0	0.0
4/6 mm aggregates [Kg/m^3]	0.0	0.0	0.0	0.0	0.0	0.0
6/10 mm aggregates [Kg/m^3]	0.0	0.0	1378.6	1066.8	0.0	0.0
10/14 aggregates [Kg/m^3]	0.0	0.0	0.0	0.0	0.0	1231.9
Total water [Kg/m^3]	119.0	144.4	106.4	135.9	162.2	81.5
Effective water [Kg/m^3]	113.6	139.1	100.8	130.5	156.7	76.5
Effective water/cement ratio	0.285	0.335	0.248	0.311	0.360	0.210
Theoretical air content calculated on cylinders [%]	24.7%	19.6%	24.6%	19.6%	14.6%	34.0%
Unconfined compressive strength at 28 days [MPa]	13.1	17.6	9.8	11.7	14.4	3.6
Water porosity [%]	27.8%	24.6%	29.3%	25.1%	19.4%	39.0%
Permeability [cm/s]	0.17	0.03	0.71	0.36	0.04	4.84

Figure 2 presents the correlation obtained between permeability and water porosity measured on the porous concrete designed for the present study.

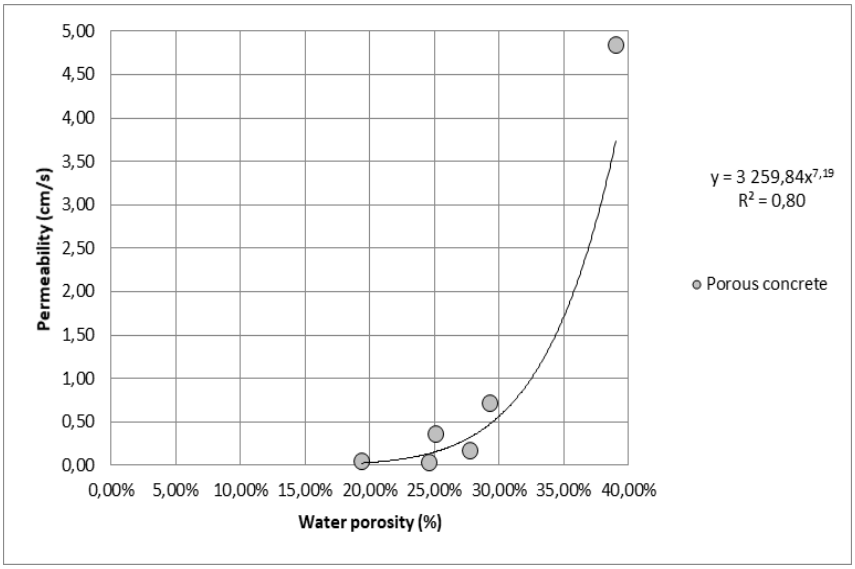

Figure 2 – Curve permeability vs porosity

The permeability was measured thanks to a vertical permeability according NF EN 12697-19 European standard. The water porosity was measured comparing the dry specimen weight after 24h in oven with the saturated weight after a 24h immersion. As expected, a correlation was observed between permeability and water porosity for this specific set of data. It allowed to achieve the mix design of porous concrete presenting a 4.84 cm/s permeability and a 3.6 MPa unconfined compressive strength. This specific mix design has been used for the prototype.
A specific concrete mortar made of fine elements (0/2 sand) was also designed in order to maximize waterproofing, ensure a plane surface to place the PV cells and ensure bonding between the porous concrete and the concrete base. The choice of a cementitious material was also made to maximize the heat transfer between the layers. The mix design was driven by the need of a sufficient workability of the material without clogging of the porous concrete.
For the construction of the prototype, the cement base was produced first. After about a week of setting, the layers of porous concrete and the two layers of mortar were all cast at once (fresh on fresh state) to ensure bonding between the layers. In order to ensure the aimed porosity and by the way the permeability determined at the previous stage, the density of the porous concrete was controlled by weighting the material poured into the given prototype volume. The compaction was made manually with hammer blows on a wood plate.

4. EXPERIMENTAL SET-UP FOR THE ENERGY HARVESTING EVALUATION

One of the main objective is to evaluate the harvested energy of the prototype. For this purpose, a specific bench test has been constructed. The idea is to simulate the sunlight radiation in lab-condition, measure the temperature changes in the porous concrete and calculate the increase of the water temperature flowing through the prototype.
The equipment is composed of an halogen lamp of 1500 W, placed 1.1m above the prototype, a pyranometer to monitor the radiation of the lamp, a waterproof mold to host the prototype, two water collectors and a tank. At first, the water accumulates into the first collector, placed at the inlet of the prototype. Due to the slope of the mold (around 1%), the water flows through the porous medium until the second collector, placed at the outlet of the prototype. Via gravity, the water reaches the tank, in which a heat exchanger is able to adjust the temperature of the water at 20°C. Here, a pump reinjects the water in the collector of the inlet, and the cycle begins again.
The water flow of the pump is regulated so that the water does not overflow from the collector. In particular, the cycle is in equilibrium when the hydraulic load ΔH is constant during time (Figure 3).

When the bench test is full operative, the water passes through the porous concrete, which is at higher temperature because of the lamp radiations. Hence, the water warms up thanks to the convection with the concrete.
The changes in temperature are detected by 8 sensors: 3 placed in the top mortar (interface mortar-solar cell); 3 in the bottom mortar and 2 placed in the inlet and the outlet tanks of the prototype.

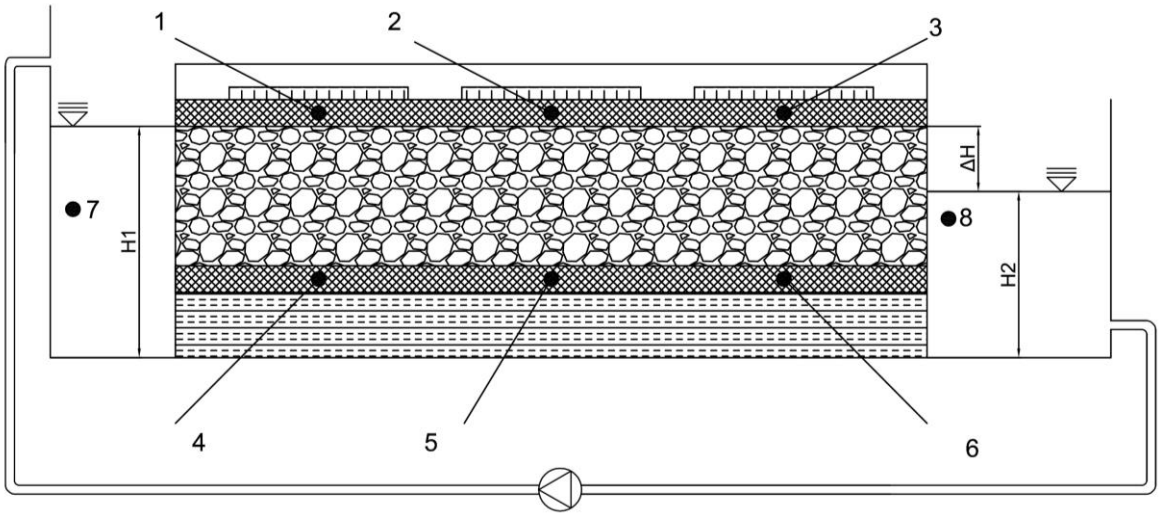

Figure 3 – General overview of the prototype. On the left the inlet of water, on the right the outlet. Black dots indicate the positions of the thermocouples

The measurements of the sensors are recorded each 5 minutes by a multi-channel data-logger.
At the same time, the electric output of the solar cells is given by an in-house measurements system, which simultaneously detects the intensity and the voltage. The row data are registered in a dedicated pc throughout the test.

5. RESULTS

The test is performed in quasi-permanent regime (constant radiation illumination of 1000 W/m^2) and in two conditions: absence of water flow and presence of water flow.
The objective is to understand if concrete and solar cells can both benefit of the cooling effect of the water.

5.1 Absence of water flow

In road pavement, the dominant heat transfer mode is radiation/convection at the top layer and convection/conduction through the porous concrete (Venkatasubramanian, 1964), (Barisic et al., 2022). Assuming that the pavement is layered system, the heat equation is given by (Chen et al., 2019):

$$\frac{k_i}{\rho_i c_i}\frac{\partial^2 T_i(x,t)}{\partial x^2} = \frac{\partial T_i(x,t)}{\partial t} \qquad (1)$$

Where:

- T_i is the temperature in the i-th layer [°C]
- K_i is the thermal conductivity of the i-th layer [W/mK]
- ρ_i is the density of the i-th layer [kg/m^3]
- c_i is the specific heat of the i-th layer [J/Kg·K]

The boundary condition is given by the energy balance of the pavement. For example, in the interface concrete/semi-transparent layer, the boundary condition can be written as:

$$k_c \frac{\partial T_c(x,t)}{\partial t} = q_{ns} - q_{nl} - q_c \qquad (2)$$

Where:

- q_{ns} is the net solar radiation, filtered from the transparent layer and absorbed by the concrete layer;
- q_{nl} is the net long-wave radiation emitted from the concrete;
- q_c is the heat flux induced by convection between the concrete and the air in the pores.

In this context, the authors first measured the temperature variations of the prototype, in absence of water flow (Figure 4).
The pyranometer detects a tension between 0.006 and 0.007 V. It proves that the radiation is in quasi-static regime. The small voltage variations are probably due to some internal disturbance of the device.

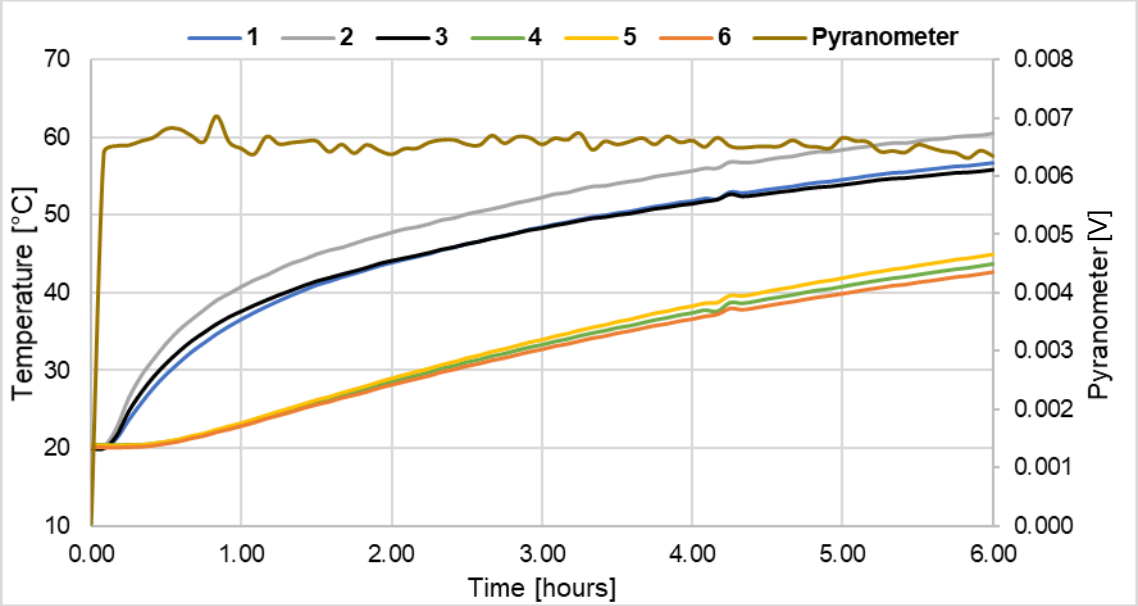

Figure 4 – Experimental temperature variations in absence of water flow

The highest temperature is detected by the thermocouple 2, because it is placed in the top concrete mortar along the vertical between the lamp and the surface. The thermocouples 1 and 3 detect the same temperature, because they are placed at the same distance from the lamp. The temperature of the thermocouples 4, 5 and 6, placed in the bottom mortar, drops proportionally to the thickness and inversely to the thermal conductivity of the concrete.
At 6 hours, the highest temperature is 60.5 °C, while the lowest is 42.6 °C. Furthermore, the trends of the curves suggest that the prototype is not yet in equilibrium. This is because the prototype has high thermal inertia, which represents the degree of slowness with which the temperature reaches that of the environment (Lizarraga & Picallo-Perez, 2020). In other terms, the energy balance between prototype and surrounding is not yet constant with respect to the time. This condition can be expressed as:

$$k_c \frac{\partial T_c(x, t = 6h)}{\partial t} < k_c \frac{\partial T_c(x, t = 6h + dt)}{\partial t} \qquad (3)$$

5.2 Presence of water flow

In presence of water flow, the prototype benefits of the cooling effect of the water. As shown in Figure 5, all the thermocouples measure lower temperatures in comparison to the previous test without water flow. More in detail, at 6 hours, the highest temperature is 34°C, while the lowest is 23.2 °C (around 1.8 times lower than the case without water).

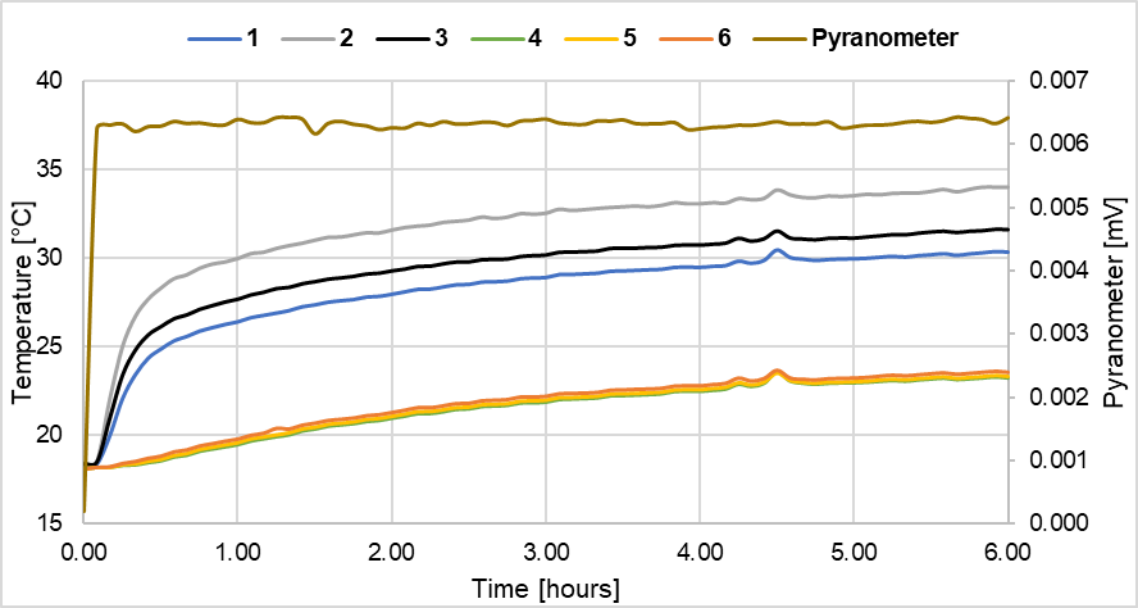

Figure 5 – Experimental temperature variations in presence of water flow

The highest temperatures are detected by the thermocouple 2, because it is the most close to the solar radiation source. Among the others thermocouples placed in the top mortar, the 1 detects the lowest temperatures, because it is placed nearby the inlet. This area is better water-saturated than the outlet, enhancing the heat exchanges between water and concrete.
No difference is observed in the measurements of the thermocouples 4, 5 and 6, because they are placed at the bottom side of the prototype, which is always full water-saturated.
The little pick observed at around 4h:30 is probably due to the interference of external sun radiation, coming from a window beside the test bench.
Contrary to what is seen in Figure 4, the curves seem to stabilize, because the prototype is reaching the equilibrium. In equation (2), we can add a 4th contribution due to the convection between water and concrete. In other terms, the energy balance between surrounding and prototype tends to be constant with respect to time.
Regarding the harvested energy, it depends on the rise of the water temperature between inlet (thermocouple 7) and outlet (thermocouple 8). The equation is:

$$E = \rho_f \cdot C_{p,f} \cdot Q \cdot \Delta T \qquad (4)$$

Where:

- ρ_f is the density of the fluid, [kg/m^3] (≈ 1000 Kg/m3 for the water),
- $C_{p,f}$ is the specific heat capacity of the fluid, J/Kg·K (≈ 4180 J/Kg·K for the water);
- Q is the waterflow through the porous concrete, [m^3/s],
- ΔT is the difference of temperature between the outlet and the inlet of the prototype, [K].

Q is measured when the prototype is working at full capacity and it is in equilibrium. For a slope of 1%, the water flow is 0.0335 m^3/s.

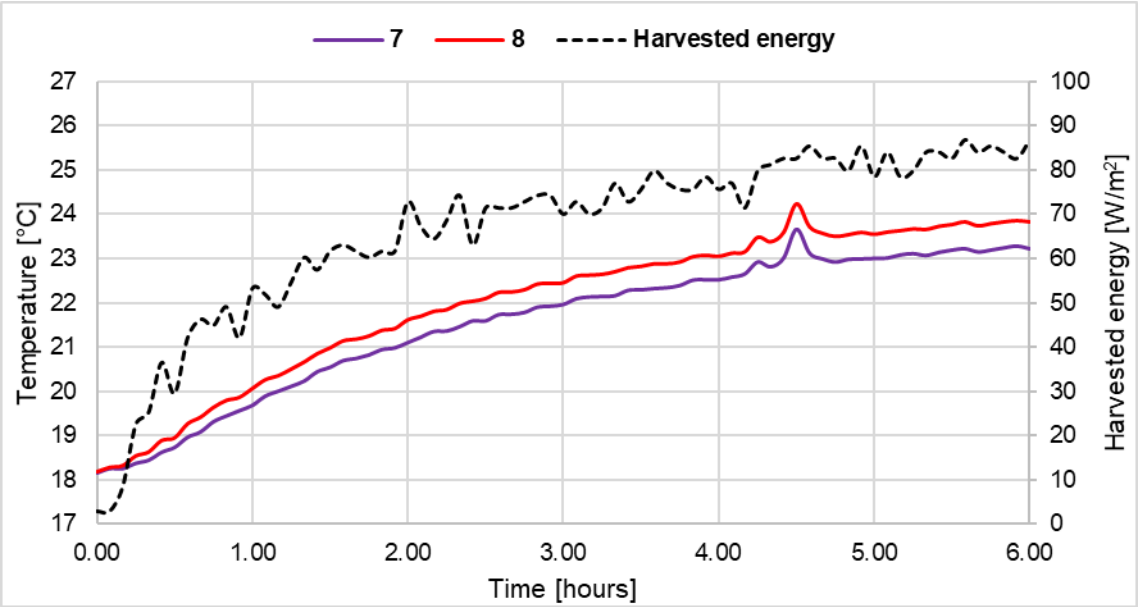

Figure 6 – Harvested energy of the porous concrete

It is worth noting that the temperature detected by the thermocouple 7 is not 20°C as in the tank, but it ranges between 18.2 °C and 23.2 °C. This slight variation is probably due to the poor thermal insulation of the pump and of the inlet collector. Furthermore, the entire experimental set-up tends to heat up with the time during the test. This would explain the increase of temperature up to 23.2 °C.
During the first 30 minutes, the harvested energy increases quickly, because the prototype tends to heat up more over this time interval. After 3 hours, the harvested energy is more stable and it ranges between 70 and 85 Watt (Figure 6).
The average value at 6 h is 66.3 W. The solar radiation intercepted from the surface of the prototype is around 110 W; consequently, the thermal efficiency is around 60%.
In comparison to the state of art, the concrete has, on average an efficiency 58% higher than the porous asphalt.

5.3 Electric output of the solar cell

As it is well known, the efficiency of a solar cell is inversely proportional to its temperature.
The previous results demonstrated how the water flow is able to relieve the temperature of the prototype concrete. Consequentially, also the solar cell should benefit of this “cooling effect”. To confirm the latter, the maximum power point of the solar cell has been monitored for 6 hours, at 1000 W/m^2, with and without water flow.
The maximum power point is the highest power delivered at a given irradiance and temperature. It represents the maximum of the product between intensity and voltage of the solar cell.

$$MPP = \max[V \cdot I] \qquad (5)$$

Intensity and voltage are simultaneously detected by an in-house measurement system, while a dedicated software is able to track the so-called “Intensity-Voltage curve” each 5 minutes.
The measurements of MPP refer to a single solar cell, placed at the centre of the prototype. Due to the absorption/reflection of the solar radiation by the semi-transparent layer, the MPP undergoes a certain reduction, depending on the thickness of the top layer, the transparency of the glue, of the glass aggregates and the presence of fine particles.
In Table 6, the measurements of MPP are differentiated in terms of presence and absence of water flow and they refer at:

- t =0 hours, when the temperature of the prototype corresponds to the ambience temperature (around 18°C);

- t =6 hours, when the temperature of the prototype is affected by the continuous exposition to the lamp radiation.

Table 6 – Measurements of Maximum Power Point

	MPP(t=0 hours) [Watt]	**MPP (t = 6 hours) [Watt]**	**MPP_{loss} [Watt]**	**MPP_{loss} [%]**
Water flow	0.890	0.875	0.015	1.7
No water flow	0.948	0.882	0.066	7.0

The results show that the water has a cooling effect on the solar cell, which translates into a MPP_{loss} of just 1.7 % after 6 hours of exposition to the lamp radiation. If the water is not flowing, the MPP_{loss} can reach the 7%.

CONCLUSIONS

This paper investigates the use of porous concrete for the extraction of heat energy through the road infrastructure. The innovation is merging a photovoltaic road with a porous concrete in order maximize the harvested energy. The idea is to add novel functionalities to the road, as moderating the negative effects of extreme events thanks to the temperature control.
More in detail, the authors designed a porous mixture, characterized by high porosity and high permeability.
The objectives are: i) evaluating the variations of the temperature in the prototype in presence and absence of water flow; ii) quantifying the cooling effect of the water thanks to the concrete layer; iii) calculating the harvested heat energy and iv) understanding if the solar cell can benefit of the cooling effect.
Based on the experimental results, the following conclusions can be drawn:

- in general, the heat exchange between water and concrete has a cooling effect on the entire prototype;
- the cooling effect has the potential to counteract the heat island effect in urbanized area;
- the water decreases the gradient temperature of the pavement, reducing the curling phenomenon (curvature induced in the concrete pavement because of the difference of temperature between top and bottom);
- in absence of water flow and after 6 hours of exposition to the lamp radiation, the temperature of the concrete surface reaches a maximum of 60.5°C. Thanks to the water flow, that temperature is reduced by 1.8 times;
- in terms of harvested energy, the porous concrete has a thermal efficiency of 60%, which is around 1.6 higher than the average efficiency of the asphalt mixture;
- the efficiency of the solar cells is between 7.2 and 7.8%, which can increase the total efficiency of the prototype up to 67.8%;
- the cooling effect has a positive impact on the efficiency of the solar cell. After 6 hours, the maximum power point of the solar cell is just reduced by 1.7%, against 7% when the water is not circulating in the porous medium;

In conclusion, the hybrid solution is able to alleviate the negative effects of high temperatures on the efficiency of the solar cells, to stock part of the thermal heat through the water and to reduce the temperature of the entire structure.
Recently, a prototype of $2m^2$ has been constructed and equipped with thermocouples and heat flux sensors. The next step will be the validation of the prototype in operating outdoor conditions.

REFERENCES

AO, Khoja; Waheeb, Sa (2016) ‘Exploring the Potentials of Asphalt Solar Collectors in Hot Humid Climates’. Innovative Energy & Research, Vol 5(2): 141

ASFOUR, Sarah (2016) “Récupération d'énergie dans les chaussées pour leur maintien hors gel” PhD thesis, Université Blaise Pascal - Clermont-Ferrand II.

ASFOUR, Sarah; Frédéric, Bernardin; Evelune Toussaint; Jean-Michel, Piau (2016) ‘Hydrothermal Modeling of Porous Pavement for Its Surface De-Freezing’. Applied Thermal Engineering 107: 493–500

BARISIC, Ivana; Ivanka, Netinger, Grubeša; Hrvoje, Krstić; Dalibor, Kubica (2022) ‘Field and Laboratory Assessment of Different Concrete Paving Materials Thermal Behavior’. Sustainability 14(11): 6638

CHEN, Jiaqi; Hao, Wang; Pengyu, Xie (2019) ‘Pavement Temperature Prediction: Theoretical Models and Critical Affecting Factors’. Applied Thermal Engineering 158: 113755

GAO, Qing; Huang, Yong; Li, Ming; Liu, Yan; Yan, Yuying (2010) ‘Experimental Study of Slab Solar Collection on the Hydronic System of Road’. Solar Energy 84(12): 2096–2102

GIELEN, Dolf; Boshell, Francisco; Saygin, Deger; Bazilian, Morgan, D.; Wagner, Nicholas; Gorini, Ricardo (2019) ‘The Role of Renewable Energy in the Global Energy Transformation’. Energy Strategy Reviews 24: 38–50

HU, Hengwu; Vizzari, Domenico; Xudong, Zha; Roberts, Ronalds (2021) ‘Solar Pavements: A Critical Review’. Renewable and Sustainable Energy Reviews 152: 111712

MEIJER, Johan R; Huijbregts, Mark A. J.; Kees, C., G., J., Schotten; Aafke, M., Schipper (2018) ‘Global Patterns of Current and Future Road Infrastructure’. Environmental Research Letters 13(6): 064006

PASCUAL-MUNOZ, Pablo; Castro-Fresno, Daniel; Serrano-Bravo, Pedro; Alonso-Estébanez, Alejandro (2013) ‘Thermal and Hydraulic Analysis of Multilayered Asphalt Pavements as Active Solar Collectors’. Applied Energy 111: 324–32.

SHAOPENG, Wu; Chen, Mingyu; Zhang, Jizhe (2011) ‘Laboratory Investigation into Thermal Response of Asphalt Pavements as Solar Collector by Application of Small-Scale Slabs’. Applied Thermal Engineering 31(10): 1582–87

LE TOUZ, Nicolas; Dumoulin, Jean; Piau, Jean-Michel (2018) ‘Multi-Physics Fem Model of Solar Hybrid Roads for Energy Harvesting Performance Evaluation in Presence of Semi-Transparent or Opaque Pavement Surface Layer’. In , 6p. https://hal.inria.fr/hal-01891242

LEWIS (2005) “Basic Research Needs For Solar Energy Utilization”. Renée M. Nault, Argonne National Laboratory

LIZARRAGA, José, M., P.; Picallo-Perez, Ana (2020) “Exergy Analysis and Thermoeconomics of Buildings” .Design and Analysis for Sustainable Energy Systems, Pages 263-343

SIEBERT, Nicolas; Zacharakis, Eleftherios (2010) “Asphalt Solar Collector and Borehole Storage Design study for a small residential building area”. Master’s Thesis, Report No. E2010:11

SONEBI, Mohammed; Bassuoni, Mohammed; Yahia, Ammar (2016) “Pervious Concrete: Mix Design, Properties and Applications”. RILEM Technical Letter 1: 109-115 (DOI: http://dx.doi.org/10.21809/rilemtechlett.2016.24

VAN BIJSTERVELD, W., T.; Houben, L., J., M.; Scarpas, A.; Molenaar, A., A., A. (2001) ‘Using Pavement as Solar Collector: Effect on Pavement Temperature and Structural Response”. Transportation Research Record, 1778. https://trid.trb.org/view/717360

VENKATASUBRAMANIA, V. (1964) “Temperature Variations in a Cement Concrete Pavement and the Underlying Subgrade”. Record 60, pp 15-27

VIZZARI, Domenico; Chailleux, Emmanuel; Lavaud, Stéphane; Gennesseaux, Eric; Bouron, Stéphane (2020) “Fraction Factorial Design of a Novel Semi-Transparent Layer for Applications on Solar Roads”. Infrastructures 2020, 5(1), 5; https://doi.org/10.3390/infrastructures5010005

VIZZARI, Domenico; Gennesseaux, Eric; Lavaud, Stéphane; Bouron, Stéphane; Chailleux, Emmanuel (2021) ‘Pavement Energy Harvesting Technologies: A Critical Review’. RILEM Technical Letters 6: 93–104

VIZZARI, Domenico; Gennesseaux, Eric; Lavaud, Stéphane; Bouron, Stéphane; Chailleux, Emmanuel (2021) “Surface Dressing Treatment for Applications on Solar Roads,” ISBM 2020: Proceedings of the RILEM International Symposium on Bituminous Materials 1719–1725, https://doi.org/10.1007/978-3-030-46455-4_218

YAN, Liu; Gao, Qing; Huang, Yong (2009) ‘Modeling Hydronic Solar Collection on Slab of Road and Bridge and a Feature Study’. In 2009 International Conference on Energy and Environment Technology, 733–36